Analysis and Design of Microstrip-Slot Line for Phase Shifting Applications

EL-BADAWY EL-SHARAWY, MEMBER, IEEE, AND ROBERT W. JACKSON, SENIOR MEMBER, IEEE

Abstract — **This paper describes the analysis and design of printed phase shifters based on the microstrip-slot line and, as a special case, the microstrip line. A spectral-domain analysis is presented where the necessary Green's functions are formulated using the transmission matrix technique. The nonreciprocal characteristics for single and multilayer structures are studied. Microstrip-slot in a multilayer structure of ferrite and high-dielectric material is found to have considerably more nonreciprocity than microstrip-slot or microstrip in a single layer structure. Over 65°/cm is predicted for certain optimized designs. This, in addition to the 50 Ω design capability of the line, make the microstrip-slot line a suitable choice for phase shifting applications. A multilayer microstrip-slot line was constructed on a rectangular ferrite toroid. Differential phase shifts of roughly 45°/cm were measured over a 6.0–8.5 GHz frequency range. These results are in good agreement with the analysis.**

I. Introduction

RECENTLY, printed phase shifters have received renewed interest due to their many attractive features. This type of phase shifter is easy to construct, is relatively low in cost, and can be compatible with coaxial feeds and integrated circuits. The objective of published work [1], [2] on printed phasers has been primarily to increase the available nonreciprocity. Multilayer structures of ferrite and medium- or high-permittivity materials have been suggested for this purpose. Most of these studies have been confined to lines with inherently elliptic fields such as slot line and coplanar waveguide [1]–[4]. Other types of printed phase shifters such as the microstrip line have not generated similar interest owing to their weak nonreciprocity [3]. Several theories on the nonreciprocal microstrip line have been published [5]–[8], but none have been verified experimentally. Furthermore, an obvious disagreement between different theories [5], [7] has been reported [7].

The microstrip-slot line phaser, shown in Fig. 1, is a modification of the coplanar waveguide phaser [4]. Its advantages over coplanar waveguide include a 50 Ω impedance, enhanced compatibility with microstrip, and, in the multilayer case, increased nonreciprocity. The microstrip-slot line on dielectric substrates was studied in [9]. However, to date no experimental or theoretical work has been reported on the microstrip-slot line on ferrite substrates.

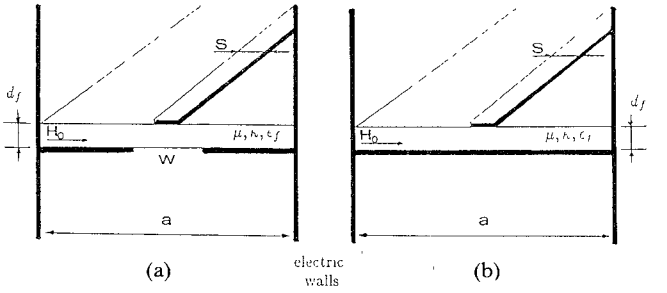

Fig. 1. Geometry of (a) microstrip-slot lines and (b) microstrip.

This paper presents a rigorous analysis of the microstrip-slot line on ferrite substrates. The analysis is formulated in the spectral domain using the transmission matrix technique [4]. Single-layer structures were considered first because of their simplicity. The analysis for single-layer structures is checked by comparison with published experimental and theoretical results for the microstrip line [7], [8], [10]. Microstrip-slot lines in various multilayer structures are then studied and compared with respect to their nonreciprocity, impedance, and frequency response. Experimental measurements of a multilayer microstrip-slot line are presented and compared with calculations.

In this paper, the Green's function formulation is described in Section II, followed by a brief outline of the moment method solution in Section III. Then, the nonreciprocal characteristics of single and multilayer structures are described in Section IV. Finally, the nonreciprocal phase measurements of a multilayer structure are presented in Section V and the paper is concluded in Section VI.

II. Green's Function Formulation

In this section, a Green's function in the spectral domain is formulated for multilayer microstrip-slot line structures. The formulation is based on the transmission matrix technique [4] extended to include two sources, an electric field source and an electric current source. We start by considering a single slab, shown in Fig. 2, defined

Manuscript received July 24, 1989; revised October 17, 1989. This work was supported by the Special Microwave Device Operation of the Raytheon Company, Northborough, MA.

R. W. Jackson is with the Department of Electrical and Computer Engineering, University of Massachusetts, Amherst, MA 01003.

E. El-Sharawy was with the Department of Electrical and Computer Engineering, University of Massachusetts, Amherst, MA. He is now with the Department of Electrical and Computer Engineering, Arizona State University, Tempe, AZ 85287.

IEEE Log Number 8932999.

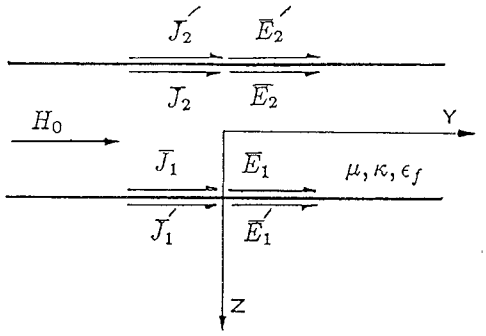

Fig. 2. Fields and currents on a single ferrite slab.

by its transmission matrix [4] as

$$\begin{bmatrix} \tilde{\tilde{E}}_2 \\ \tilde{\tilde{J}}_2 \end{bmatrix} = \tilde{\tilde{T}} \begin{bmatrix} \tilde{\tilde{E}}_1 \\ \tilde{\tilde{J}}_1 \end{bmatrix} = \begin{bmatrix} \tilde{\tilde{T}}_E & \tilde{\tilde{Z}}_T \\ \tilde{\tilde{Y}}_T & \tilde{\tilde{T}}_J \end{bmatrix} \begin{bmatrix} \tilde{\tilde{E}}_1 \\ \tilde{\tilde{J}}_1 \end{bmatrix} \tag{1}$$

where $\tilde{\tilde{E}}_1$, $\tilde{\tilde{E}}_2$ are the tangential electric fields at the boundaries of the layer, $\tilde{\tilde{J}}_1$, $\tilde{\tilde{J}}_2$ are the surface tangential currents defined by $\tilde{\tilde{J}}_i = \hat{z} \times \tilde{\tilde{H}}_i (i = 1,2)$, $\sim$ denotes the Fourier transform with respect to the x and y directions, and $\tilde{\tilde{H}}_i$ is the tangential magnetic field just inside the slab being considered (Fig. 2). The other currents in Fig. 2, $\tilde{\tilde{J}}_1'$ and $\tilde{\tilde{J}}_2'$, are the currents due to fields in the upper and lower semispaces (above surface 2 and below surface 1, respectively). In the simple case of semi-infinite space on both sides of the slab, these currents can be written as

$$\tilde{\tilde{J}}_1' = \tilde{\tilde{\bar{G}}}_1 \tilde{\tilde{E}}_1' \tag{2a}$$

$$\tilde{\tilde{J}}_2' = \tilde{\tilde{\bar{G}}}_2 \tilde{\tilde{E}}_2' \tag{2b}$$

where $\tilde{\tilde{J}}_i' = \hat{n}_i \times \tilde{\tilde{H}}_i'$, $\hat{n}_i$ is the unit vector normal to the ith surface ($\hat{n}_1 = \hat{z}$, $\hat{n}_2 = -\hat{z}$), and $\tilde{\tilde{\bar{G}}}_i$ is given in Appendix I.

The total surface currents $\tilde{\tilde{J}}_{S1}$, $\tilde{\tilde{J}}_{S2}$ can be written in terms of $\tilde{\tilde{J}}_1$, $\tilde{\tilde{J}}_2$, $\tilde{\tilde{J}}_1'$, $\tilde{\tilde{J}}_2'$ as

$$\tilde{\tilde{J}}_{S1} = \hat{z} \times \left(\tilde{\tilde{H}}_1' - \tilde{\tilde{H}}_1 \right) = \tilde{\tilde{J}}_1' - \tilde{\tilde{J}}_1 \tag{3a}$$

$$\tilde{\tilde{J}}_{S2} = \hat{z} \times \left(\tilde{\tilde{H}}_2 - \tilde{\tilde{H}}_2' \right) = \tilde{\tilde{J}}_2 + \tilde{\tilde{J}}_2'. \tag{3b}$$

From (1), (2), and (3), a 4×4 Green's function, $\tilde{\tilde{\bar{G}}}$, can be shown to be (Appendix II)

$$\begin{bmatrix} \tilde{\tilde{J}}_{S1} \\ \tilde{\tilde{E}}_2 \end{bmatrix} = \tilde{\tilde{\bar{G}}} \begin{bmatrix} \tilde{\tilde{E}}_1 \\ \tilde{\tilde{J}}_{S2} \end{bmatrix} = \begin{bmatrix} \tilde{\tilde{\bar{G}}}^Y & \tilde{\tilde{\bar{G}}}^J \\ \tilde{\tilde{\bar{G}}}^E & \tilde{\tilde{\bar{G}}}^Z \end{bmatrix} \begin{bmatrix} \tilde{\tilde{E}}_1 \\ \tilde{\tilde{J}}_{S2} \end{bmatrix}$$

$$= \begin{bmatrix} \tilde{\tilde{\bar{G}}}_1 + \left(\tilde{\tilde{T}}_J + \tilde{\tilde{\bar{G}}}_2 \tilde{\tilde{Z}}_T \right)^{-1} \left(\tilde{\tilde{Y}}_T + \tilde{\tilde{\bar{G}}}_2 \tilde{\tilde{T}}_E \right) & -\left(\tilde{\tilde{T}}_J + \tilde{\tilde{\bar{G}}}_2 \tilde{\tilde{Z}}_T \right)^{-1} \\ \tilde{\tilde{T}}_E - \tilde{\tilde{Z}}_T \left(\tilde{\tilde{T}}_J + \tilde{\tilde{\bar{G}}}_2 \tilde{\tilde{Z}}_T \right)^{-1} \left(\tilde{\tilde{Y}}_T + \tilde{\tilde{\bar{G}}}_2 \tilde{\tilde{T}}_E \right) & \tilde{\tilde{Z}}_T \left(\tilde{\tilde{T}}_J + \tilde{\tilde{\bar{G}}}_2 \tilde{\tilde{Z}}_T \right)^{-1} \end{bmatrix} \begin{bmatrix} \tilde{\tilde{E}}_1 \\ \tilde{\tilde{J}}_{S2} \end{bmatrix} \tag{4}$$

where $\tilde{\tilde{\bar{G}}}^Y, \tilde{\tilde{\bar{G}}}^Z, \tilde{\tilde{\bar{G}}}^E, \tilde{\tilde{\bar{G}}}^J$ are 2×2 submatrices of $\tilde{\tilde{\bar{G}}}$. This hybrid Green's function is required in a full-wave solution for the microstrip-slot where slot currents and microstrip fields are expressed as a function of slot fields and microstrip currents as in (4).

When an additional layer is placed below or above the slab in Fig. 2, then $\tilde{\tilde{\bar{G}}}_1$ or $\tilde{\tilde{\bar{G}}}_2$ in (2) is replaced by the function

$$\tilde{\tilde{\bar{G}}}_{Si} = \left(\tilde{\tilde{Y}}_{Ti} + \tilde{\tilde{T}}_{Ji} \tilde{\tilde{\bar{G}}}_i \right) \left(\tilde{\tilde{T}}_{Ei} + \tilde{\tilde{Z}}_{Ti} \tilde{\tilde{\bar{G}}}_i \right)^{-1} \tag{5}$$

where $i = 1$ or 2 and $\tilde{\tilde{Y}}_{Ti}$, $\tilde{\tilde{T}}_{Ji}$, $\tilde{\tilde{T}}_{Ei}$, $\tilde{\tilde{Z}}_{Ti}$ are the transmission submatrices of the layer added to the lower or upper side. To find the Green's functions for the new case, $\tilde{\tilde{\bar{G}}}_i$ in (4) are replaced by the new semispace Green's functions $\tilde{\tilde{\bar{G}}}_{Si}$.

In a general case where multiple layers of ferrite or dielectric may exist above the microstrip, between the microstrip and the slot, or below the slot, the transmission matrix of a group of layers can be found by taking the product of the transmission matrices of the individual layers. The resulting matrix can then be used in (4) and (5) to find Green's functions.

Green's functions for the special case of a microstrip line can be found by imposing the boundary condition $\tilde{\tilde{E}}_1 = 0$ in (4). The resulting Green's function is

$$\tilde{\tilde{\bar{G}}}^{MS} = \tilde{\tilde{Z}}_T \left(\tilde{\tilde{T}}_J + \tilde{\tilde{\bar{G}}}_2 \tilde{\tilde{Z}}_T \right)^{-1} = \left(\tilde{\tilde{\bar{G}}}_2 + \tilde{\tilde{T}}_J \tilde{\tilde{Z}}_T^{-1} \right)^{-1}. \tag{6}$$

Equations (4) and (6) show the usefulness of the transmission matrix approach in simplifying the formulation of the Green's function. Formulating the Green's function using other techniques (such as the boundary condition formulation) can be cumbersome and will result in lengthy expressions. On the other hand, the availability of transmission matrices for ferrite and dielectric layers [4] makes it possible to formulate Green's functions in a high level manner.

III. Full-Wave Formulation

The geometry of the microstrip-slotline with electric sidewalls is shown in Fig. 1. For infinitely long structures with a wave traveling in the x direction, the x dependence can be assumed to be $e^{-j\beta x}$. This, in addition to the

boundary conditions at the electric walls, will allow (4) to be rewritten as [4]

$$\begin{bmatrix} \bar{J}_{S1}(y) \\ \bar{E}_2(y) \end{bmatrix} = \sum_{\iota=-\infty}^{\infty} \bar{\bar{G}}(-\beta, k_{y\iota}) \begin{bmatrix} \tilde{\bar{E}}_1(k_{y\iota}) \\ \tilde{\bar{J}}_{S2}(k_{y\iota}) \end{bmatrix} e^{jk_{y\iota}y} \quad (7)$$

where $k_{y\iota} = i\pi/a$ and the fields $\tilde{\bar{E}}_1$, $\tilde{\bar{J}}_{S2}$ are constrained by

$$\tilde{E}_{x1}(k_{y\iota}) = -(-1)^{\iota}\tilde{E}_{x1}(-k_{y\iota}) \quad (8a)$$

$$\tilde{E}_{y1}(k_{y\iota}) = (-1)^{\iota}\tilde{E}_{y1}(-k_{yi}) \quad (8b)$$

$$\tilde{J}_{xS2}(k_{y\iota}) = -(-1)^{\iota}\tilde{J}_{xS2}(-k_{y\iota}) \quad (8c)$$

$$\tilde{J}_{yS2}(k_{y\iota}) = (-1)^{\iota}\tilde{J}_{yS2}(-k_{y\iota}). \quad (8d)$$

Since $\tilde{E}_{x1}$, $\tilde{J}_{xS2}$ are even functions of y and $\tilde{E}_{y1}$, $\tilde{J}_{yS2}$ are odd, i in (7) takes on only odd values. Some minor changes in the above formulation are needed for structures confined by magnetic walls. In particular, minus sign inversion will occur in (8) and as a result, i will only take on even values.

The full-wave solution for the microstrip-slot is based on the fact that both the electric fields $\bar{E}_2$ on the microstrip and the electric currents $\bar{J}_{S1}$ in the slot must vanish when β is an acceptable solution for the propagation constant. These boundary conditions can be enforced by employing Galerkin's method where fields (or currents) are expanded and tested using a common set of functions. In this work, the expansion of $\bar{E}_1$, $\bar{J}_{S2}$ takes the form

$$E_{x1}(y) = \sum_{n=0,\text{even}}^{N_{x1}} a_n f_{xn}$$

$$E_{y1}(y) = \sum_{n=1,\text{odd}}^{N_{y1}} b_n f_{yn}$$

$$J_{xS2}(y) = \sum_{n=0,\text{even}}^{N_{x2}} c_n h_{xn}$$

$$J_{yS2}(y) = \sum_{n=1,\text{odd}}^{N_{y2}} d_n h_{yn} \quad (9)$$

where f_{xn}, f_{yn}, h_{xn}, h_{yn} are the expansion functions and a_n, b_n, c_n, d_n are the constants to be determined. In this work, the following expansion functions are used:

$$f_{xn} = U_n\left(\frac{2y}{W}\right)\sqrt{1-\left(\frac{2y}{W}\right)^2} \quad (10a)$$

$$f_{yn} = T_n\left(\frac{2y}{W}\right)\Big/\sqrt{1-\left(\frac{2y}{W}\right)^2} \quad (10b)$$

$$h_{xn} = T_n\left(\frac{2y}{S}\right)\Big/\sqrt{1-\left(\frac{2y}{S}\right)^2} \quad (10c)$$

$$h_{yn} = U_n\left(\frac{2y}{S}\right)\sqrt{1-\left(\frac{2y}{S}\right)^2} \quad (10d)$$

where T_n, U_n are Chebyshev polynomials of the first and second kinds, respectively. The Fourier transforms of these basis functions are available in closed form in terms of Bessel functions [4].

The testing procedure in Galerkin's method results in a matrix, $\bar{\bar{A}}$, having a hybrid form:

$$\bar{\bar{A}} = \begin{bmatrix} \bar{\bar{Y}} & \bar{\bar{C}} \\ \bar{\bar{D}} & \bar{\bar{Z}} \end{bmatrix} \quad (11)$$

where

$$Y_{\ell m}^{pq} = \sum_{\iota=-\infty,\text{odd}}^{\infty} F_{p\ell}^*\left(\frac{i\pi}{a}\right)\tilde{G}_{pq}^{Y}\left(-\beta, \frac{i\pi}{a}\right)F_{qm}\left(\frac{i\pi}{a}\right)$$

$$C_{\ell m}^{pq} = \sum_{\iota=-\infty,\text{odd}}^{\infty} F_{p\ell}^*\left(\frac{i\pi}{a}\right)\tilde{G}_{pq}^{E}\left(-\beta, \frac{i\pi}{a}\right)H_{qm}\left(\frac{i\pi}{a}\right)$$

$$D_{\ell m}^{pq} = \sum_{i=-\infty,\text{odd}}^{\infty} H_{p\ell}^*\left(\frac{i\pi}{a}\right)\tilde{G}_{pq}^{J}\left(-\beta, \frac{i\pi}{a}\right)F_{qm}\left(\frac{i\pi}{a}\right)$$

$$Z_{\ell m}^{pq} = \sum_{\iota=-\infty,\text{odd}}^{\infty} H_{p\ell}^*\left(\frac{i\pi}{a}\right)\tilde{G}_{pq}^{Z}\left(-\beta, \frac{i\pi}{a}\right)H_{qm}\left(\frac{i\pi}{a}\right). \quad (12)$$

The indices ℓ, m refer to the order of the expansion and p, q refer to the x or y components. The functions F and H are the Fourier transforms of the functions in (10). The propagation constant can be found by adjusting β until the determinant, $|\bar{\bar{A}}|$, is forced to zero. The difference between the forward propagation constant, β_f, and the reverse propagation constant, β_r ($+x$ and $-x$ directions), is the nonreciprocal phase shift $\Delta\phi$ per unit length.

The following comments can be made about the numerical aspects of this problem. The number of basis functions N_{x1}, N_{y1}, N_{x2}, N_{y2} is increased until $\Delta\phi$ converges. In the convergence test, numerical problems were sometimes observed due to the large difference in element magnitudes of the matrix $\bar{\bar{A}}$ (elements of $\bar{\bar{Z}}$ can be 10^6–10^8 times larger than elements of $\bar{\bar{Y}}$). In this case, a normalization process of the arbitrary constants a_n, b_n, c_n, d_n was found to be effective in eliminating these problems. Also, as the slot width W increases compared to the microstrip widths ($W \geqslant 2S$), the expansion functions for the slot fields, given by (10a) and (10b), start to converge slowly. Faster convergence was possible by using an alternative set of basis functions:

$$f_{xn} = \cos\frac{(n+1)\pi y}{W} \quad (13a)$$

$$f_{yn} = \sin\frac{n\pi y}{W}. \quad (13b)$$

Note that the basis functions of (10a) and (10b) still converge faster than those of (13a) and (13b) for small slot widths ($W \leqslant S$). This is presumed to be due to the fact that the edge condition becomes an important effect for narrow slots, and thus functions which satisfy the edge condition are necessary. In contrast, when wide slots are analyzed the edge effects are relatively localized and sinusoidal functions better match the interior field structure. In

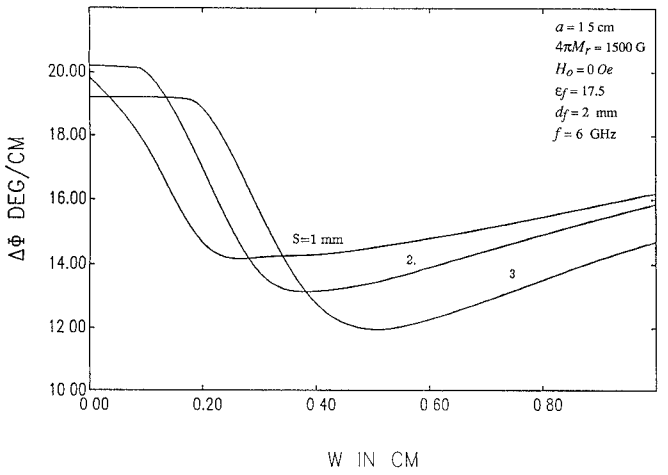

Fig. 3. Effect of microstrip-slot dimensions on differential phase shift in a single layer structure.

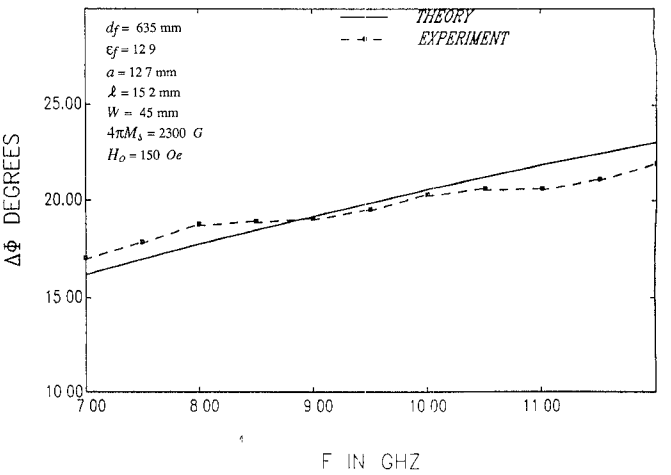

Fig. 4. Calculation and measurements [10] of a microstrip line on ferrite substrate.

most cases two longitudinal and two transverse expansion functions were used to model the slot fields, and two longitudinal and one transverse current function were used for the microstrip. In the special case of zero slot width (a solo microstrip line), only the currents on the line are expanded, and the basis functions of (10c) and (10d) result in fast convergence for all cases of interest ($S < 0.1\lambda_0$).

IV. Results

A. Single-Layer Structures

This section describes the nonreciprocal characteristics of microstrip-slot line on a single ferrite layer. These structures are simple and have the advantage of 50 Ω design capability and direct compatability with coaxial feeds.

The computed differential phase shift of the microstrip-slot line is plotted in Fig. 3 versus the slot width for various values of the microstrip width. The highest differential phase shift is obtained for $W = 0$ (the microstrip line). The differential phase starts to noticeably decrease when the slot width becomes larger than the microstrip width.

For a single ferrite layer with its top and bottom surfaces bounded by air, the transmission line will generate field ellipticities which have opposite signs on opposite substrate surfaces [4], [11]. Since the nonreciprocal phase results from the interaction between these elliptic fields and the magnetic material [3], [4], the opposite ellipticities will counteract each other and result in a low nonreciprocity. In the case of the microstrip line, the ground plane shorts one of the counteracting fields and this explains the increased nonreciprocity of the microstrip line compared with the microstrip-slot line. However, even for the microstrip line, the differential phase is still low ($\simeq 20°/\text{cm}$). Other lines such as multilayer slot line [1] and multilayer coplanar waveguide [4] have been reported to give values of $\Delta\phi$ exceeding 40°/cm.

To check the present theory for a single-layer microstrip structure, the experimental results of [10] are plotted in Fig. 4 along with the differential phase shift calculated using the methods described above. In this experimental work, a 50 Ω microstrip line was etched on 0.025 in magnesium-manganese ferrite ($4\pi M_s = 2300$ G). The microstrip line was 15.2 mm long. The substrate dimensions were $15.2 \times 12.7 \times 0.635$ mm^3 and it was magnetized by a 1-cm-long ferrite magnet. The dielectric constant was not mentioned, but can be estimated ($\epsilon_r = 12.9$) by examining the data sheets of similar materials. The microstrip width was also not mentioned, but was assumed to be 0.45 mm so as to give a 50 Ω impedance. In computing the theoretical results shown in Fig. 4 it was assumed that the magnet's fringing field was sufficient to magnetize the entire length of the ferrite substrate (15.2 mm). Also, the substrates' sidewalls ($y = \pm a/2$) are modeled as perfect magnetic walls. Under these assumptions the difference between the predicted and measured differential phase shift is within 5 percent over the entire band.

Further verification was carried out by comparing the dispersion characteristics, calculated using our theory for a shielded microstrip on a ferrite substrate, with those calculated using the available theories in the literature [5], [7], [8]. The agreement was found to be within 3 percent of the results in [7] and within 5 percent of the results in [8], whereas a large discrepancy with [5] was observed. In particular, no microstrip slow waves were found (the propagation constant of the microstrip is less than $k_0\sqrt{\epsilon_f}$). This is the same conclusion as was reached in [7].

B. Multilayer Structures

In this section, various multilayer structures of ferrite and dielectrics are investigated in an effort to improve the microstrip-slot line nonreciprocity. The addition of a dielectric layer can replace one of the aforementioned counteracting ellipticities by a coacting ellipticity [4], [11], resulting in better nonreciprocity than with only a single layer of ferrite. This layer may be added on the microstrip side or on the slot side, as shown in Fig. 5. The effects of structure a on the differential phase is plotted in Fig. 6 versus the slot width for different values of the microstrip width. For small values of W ($W < 2S$), the differential

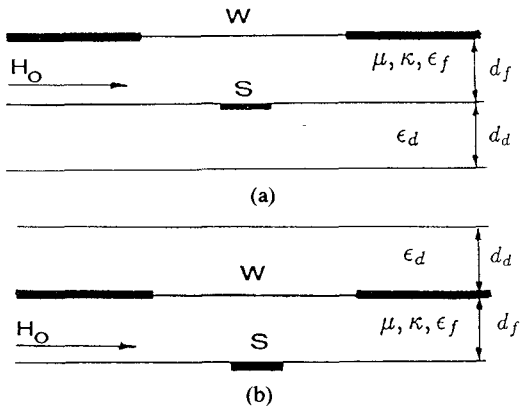

Fig. 5. Geometry of multilayer microstrip-slot line.

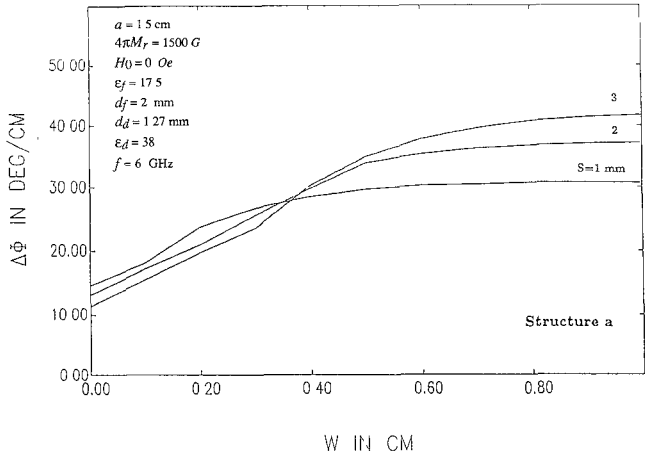

Fig. 6. Effect of microstrip-slot dimensions on differential phase shift in multilayer structure a.

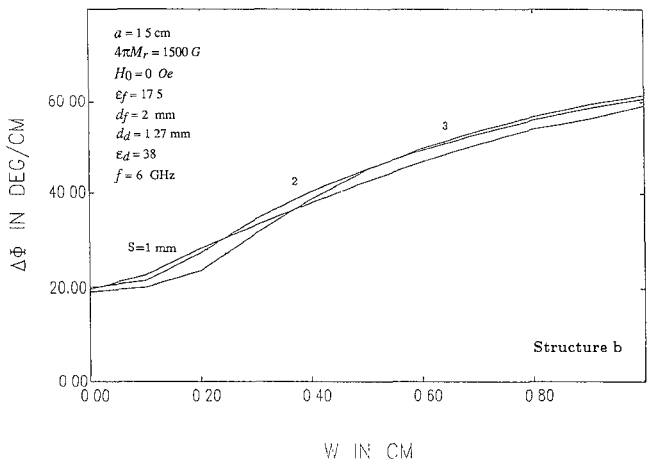

Fig. 7. Effect of microstrip-slot dimensions on differential phase shift in multilayer structure b.

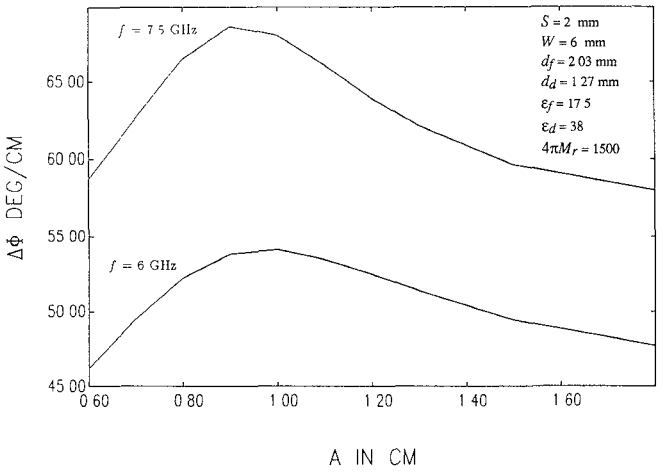

Fig. 8. Effects of sidewall separation on the microstrip-slot nonreciprocity.

phase increases with W, then starts to saturate for larger values of W. The saturation differential phase increases with the microstrip width S. As Fig. 6 shows the best nonreciprocity available from this structure was about 40°/cm, which is comparable to what has been reported for other high-performance printed phasers [1], [4] (slotline and coplanar waveguide).

In structure b, the dielectric layer is placed on the slot side. The nonreciprocity of this configuration is shown in Fig. 7. Note that the same dielectric and ferrite layers are assumed as in Fig. 6. In this configuration the differential phase does not saturate and continues to increase with the slot width W. As a result, a nonreciprocity of up to 60°/cm is available. Compared to structure a, the nonreciprocity of this structure is about 50 percent higher. Fig. 7 also shows that the differential phase has a small dependence on the microstrip width S. This will simplify the design procedure, since S can be chosen independently of the nonreciprocity considerations.

Other advantages of structure b over structure a include the feasibility of achieving a 50 Ω line impedance. This is due to the presence of air on one side of the structure b microstrip, whereas in structure a the microstrip is sandwiched between ferrite and dielectric, both having high dielectric constants. The 50 Ω design capability is necessary for direct compatability with coaxial feed. As a result, structure a will not receive any further consideration due to its relatively low nonreciprocity and low line impedance.

The nonreciprocity of structure b may be further increased by a proper choice of the electric sidewall separation. Fig. 8 shows the nonreciprocity versus the sidewall separation, a in cm, at two different frequencies, 6 GHz and 7.5 GHz. This figure shows that there is an optimum value for a, at which the nonreciprocity is maximum. This value is slightly dependent on frequency. As an example, the optimum value of a in Fig. 8 was 1.1 cm at 6 GHz and decreased slightly to 1 cm at 7.5 GHz. From Fig. 8, we also conclude that the nonreciprocity of the line increases with frequency.

The nonreciprocity of the line can be equalized over the bandwidth by adding a thin layer of low-dielectric materials as shown in Fig. 9. The effects of the new geometry on the differential phase versus frequency are shown in Fig. 10. The special case, when $t = 0$, is the structure response without the new layer. The other curves in the figure show the effect of increasing the thickness of the layer. Note that the layer thickness is still small compared to the thickness

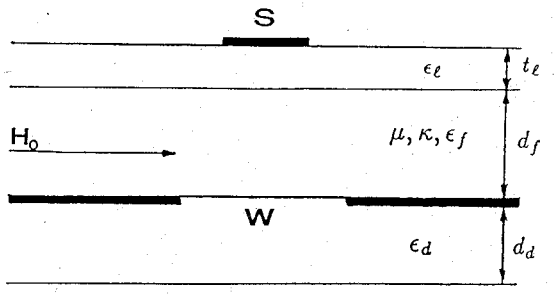

Fig. 9. Geometry of structure *b* with an additional layer of low-dielectric material.

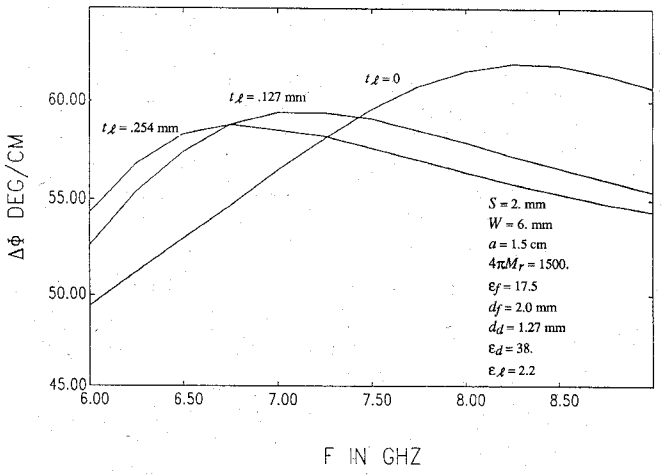

Fig. 10. Effects of the additional layer in structure *b*.

of the ferrite and the high-dielectric layers. The layer boosts the differential phase at the low end of the band shown in Fig. 10 and reduces it at the high end. As a result, a relatively flat differential phase is obtained over the band. The use of medium or high dielectric constants for the new layer was also studied and found not to be as favorable as low dielectric constants. As the dielectric constant ϵ_ℓ increases, the line nonreciprocity decreases. In addition, using low value of ϵ_ℓ makes it even easier to achieve a 50 Ω characteristic impedance.

V. Experimental Verification

In this section, we present measurements of the differential phase shift between the two latched states of a multilayer microstrip-slot line fabricated on a rectangular ferrite toroid. The outer dimensions of the toroid were $15.2 \times 10.2 \times 44.5$ mm^3 and the wall thickness was 2.03 mm. The toroid outer corners were chamfered by 0.9 mm to ensure the alignment between the magnetization and the RF fields [12]. The ferrite material had a remanent magnetization of 1500 G. The toroid outside surface was gold-plated and a 6.0-mm-wide slot was etched in the conductor on one of the two broad walls. The microstrip-slot line was formed by etching a 2.2-mm-wide microstrip on a 0.25-mm-thick piece of Duroid 5880 ($\epsilon_r = 2.2$). The microstrip was then placed inside the toroid in a manner similar to the inset of Fig. 12. To reduce the effect of the discontinuity at the coaxial input, the slot was tapered from 2.2 mm at the coax to 6.0 mm at the main microstrip-slot line, as

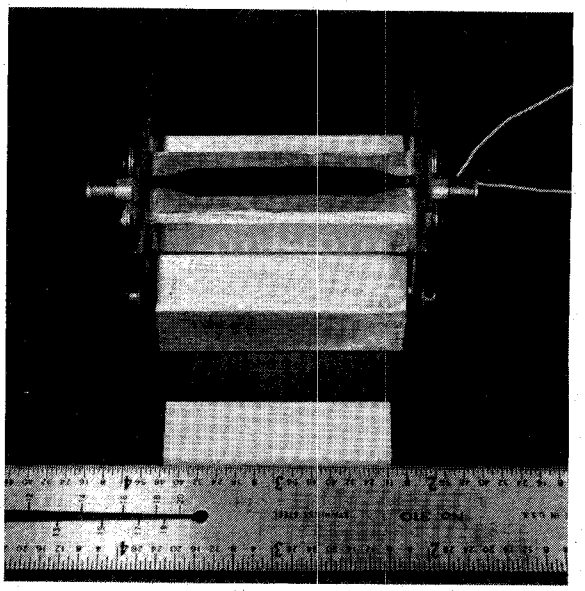

Fig. 11. Experimental structure for measurements of a multilayer microstrip-slot line.

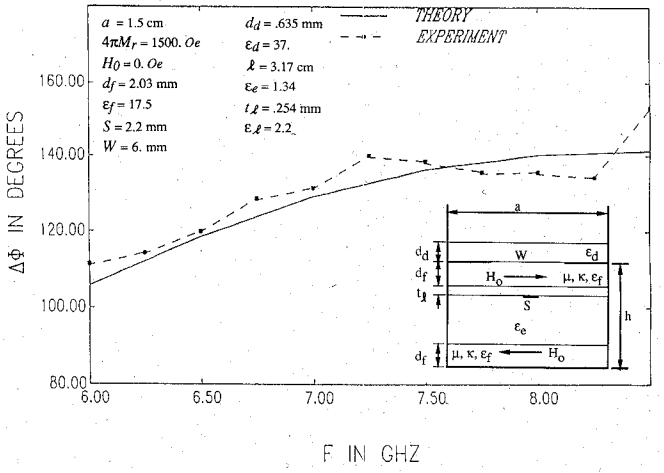

Fig. 12. Measured and calculated results of a multilayer microstrip-slot line.

shown in Fig. 11. The microstrip remained unchanged over the length (6.4 mm) of the taper. The length of the main line (where $W = 6.0$ mm) was 31.7 mm. A ceramic substrate with a dielectric constant of 37 was placed on top of the slot to form a structure similar to that shown in Fig. 5(b). The dimensions of this high-permittivity layer were $38.1 \times 11.1 \times 0.635$ mm.

The structure was theoretically modeled as shown in the Fig. 12 inset. In this figure, the ferrite toroid is modeled as two horizontal ferrite slabs between two electric walls. To approximately model the effect of the ferrite toroid's vertical sidewalls, the two horizontal slabs are separated by a dielectric layer of effective dielectric constant ϵ_e. The value of ϵ_e is calculated from the following relation [4]:

$$\epsilon_e = \left(1 - \frac{2d(\epsilon_f - 1)}{a\epsilon_f}\right)^{-1}$$

where d is the wall thickness.

Fig. 12 shows the measured differential phase and the differential phase calculated from the main line only (31.75 mm). The effects of the taper on the differential phase cannot be predicted using the present theory. However, since (a) the length and the slot width of the taper are smaller than those of the main line, and (b) the taper was partially uncovered with the high-dielectric material, the nonreciprocity of the taper will be small (see Figs. 3 and 7) and can be assumed negligible compared to the nonreciprocity of the main line. This assumption is discussed in more detail in [11].

With the previously mentioned assumption, reasonably good agreement between theory and measurements is observed. The agreement was better than 5 percent except at 8.5 GHz, where the discrepancy rose to 7 percent. Over the band of frequencies shown in Fig. 12, the return loss was about 20 dB at the low end of the band and decreased to about 12 dB at the high end. The insertion loss was about 1–2 dB.

The bandwidth was limited at the low end by magnetic losses [3]. This limits the operation of the phase shifter to frequencies higher than $\gamma 4\pi M_r/0.6 \approx \gamma 4\pi M_s$, which in this case was about 6 GHz. On the other hand, the bandwidth is limited at the high end by the excitation of higher order waveguide modes. Such modes were found to considerably increase the insertion loss of the phase shifter and reduce the accuracy and smoothness of the differential phase. The first higher order mode in the experimental structure was found to be near 8.5 GHz, which may explain the higher discrepancy between theory and measurements at this frequency.

VI. Conclusion

A rigorous analysis of the microstrip-slot line on ferrite substrate has been formulated using the transmission matrix technique. Several single-layer and multilayer structures were studied, primarily with regard to their nonreciprocal properties. Multilayer structures of ferrite and high-dielectric material were found to have the potential to combine high nonreciprocity and 50 Ω design capability. The effects of the sidewall separation have been investigated and an optimum separation was found for maximum nonreciprocity. The flatness of the differential phase was also considered. A low-dielectric layer beneath the microstrip increases the differential phase at low frequencies and decreases it at high frequencies, resulting in a flat nonreciprocity over the bandwidth. Finally, the analysis was verified by measuring the differential phase of a multilayer microstrip-slot constructed on a rectangular ferrite toroid. Good agreement between predicted and measured nonreciprocal phase was observed.

The results presented in this paper, along with the 50 Ω design capability, show the microstrip-slot to be an excellent nonreciprocal medium. However, further study of the bandwidth limitations due to the excitation of higher order modes is necessary in order to furnish a complete comparison between this transmission line and other nonreciprocal transmission lines.

Appendix I

The semispace Green's function $\bar{\bar{G}}_1$ (or $\bar{\bar{G}}_2$), in (2) can be written as

$$\bar{\bar{G}}_1 = \bar{\bar{T}}_J \bar{\bar{Z}}_T^{-1}|_{d\to\infty}. \tag{A1}$$

From the general properties of a dielectric transmission matrix [4],

$$\bar{\bar{G}}_1 = \left.\frac{\bar{\bar{T}}_J \bar{\bar{Y}}_T}{\sinh^2 kd}\right|_{d\to\infty} = \frac{jY_c}{kk_d \tanh kd} d\to\infty \left[\begin{matrix} k_y^2 - k_d^2 & -k_x k_y \\ -k_x k_y & k_x^2 - k_d^2 \end{matrix}\right]\Bigg|_{d\to\infty}. \tag{A2}$$

Taking the limit as $d \to \infty$ gives the following expression for $\bar{\bar{G}}_1$:

$$\bar{\bar{G}}_1 = \frac{jY_c}{kk_d}\left[\begin{matrix} k_y^2 - k_d^2 & -k_x k_y \\ -k_x k_y & k_x^2 - k_d^2 \end{matrix}\right] \tag{A3}$$

where

$$Y_c = \sqrt{\frac{\epsilon}{\mu_0}}$$

$$k_d = \omega\sqrt{\mu_0 \epsilon}$$

$$k = \left(k_x^2 + k_y^2 - k_d^2\right)^{1/2}.$$

Appendix II

To find $\bar{\bar{G}}$ in (4), we start by writing the currents $\tilde{\tilde{J}}_1$, $\tilde{\tilde{J}}_2$ as (see eqs. (2) and (3))

$$\tilde{\tilde{J}}_1 = \bar{\bar{G}}_1 \tilde{\tilde{E}}_1 - \tilde{\tilde{J}}_{S1} \tag{A4}$$

$$\tilde{\tilde{J}}_2 = \tilde{\tilde{J}}_{S2} - \bar{\bar{G}}_2 \tilde{\tilde{E}}_2. \tag{A5}$$

From (1), (A4), and (A5),

$$\tilde{\tilde{E}}_2 = \bar{\bar{T}}_E \tilde{\tilde{E}}_1 + \bar{\bar{Z}}_T \bar{\bar{G}}_1 \tilde{\tilde{E}}_1 - \bar{\bar{Z}}_T \tilde{\tilde{J}}_{S1} \tag{A6}$$

$$\tilde{\tilde{J}}_{S2} - \bar{\bar{G}}_2 \tilde{\tilde{E}}_2 = \bar{\bar{Y}}_T \tilde{\tilde{E}}_1 + \bar{\bar{T}}_J \bar{\bar{G}}_1 \tilde{\tilde{E}}_1 - \bar{\bar{T}}_J \tilde{\tilde{J}}_{S1}. \tag{A7}$$

Multiplying (A6) by $\bar{\bar{G}}_2$ and adding to (A7),

$$\tilde{\tilde{J}}_{S1} = \left(\bar{\bar{G}}_1 + \left(\bar{\bar{T}}_J + \bar{\bar{G}}_2 \bar{\bar{Z}}_T\right)^{-1}\left(\bar{\bar{Y}}_T + \bar{\bar{G}}_2 \bar{\bar{T}}_E\right)\right)\tilde{\tilde{E}}_1 - \left(\bar{\bar{T}}_J + \bar{\bar{G}}_2 \bar{\bar{Z}}_T\right)^{-1} \tilde{\tilde{J}}_{S2}. \tag{A8}$$

From (A6) and (A8),

$$\tilde{\tilde{E}}_2 = \left(\bar{\bar{T}}_E - \bar{\bar{Z}}_T\left(\bar{\bar{T}}_J + \bar{\bar{G}}_2 \bar{\bar{Z}}_T\right)^{-1}\left(\bar{\bar{Y}}_T + \bar{\bar{G}}_2 \bar{\bar{T}}_E\right)\right)\tilde{\tilde{E}}_1 + \bar{\bar{Z}}_T\left(\bar{\bar{T}}_J + \bar{\bar{G}}_2 \bar{\bar{Z}}_T\right)^{-1} \tilde{\tilde{J}}_{S2}. \tag{A9}$$

Therefore, $\overline{\overline{G}}$ can be written as

$$\overline{\overline{G}} = \begin{bmatrix} \overline{\overline{G}}_1 + \left(\overline{\overline{T}}_J + \overline{\overline{G}}_2\overline{\overline{Z}}_T\right)^{-1}\left(\overline{\overline{Y}}_T + \overline{\overline{G}}_2\overline{\overline{T}}_E\right) & -\left(\overline{\overline{T}}_J + \overline{\overline{G}}_2\overline{\overline{Z}}_T\right)^{-1} \\ \overline{\overline{T}}_E - \overline{\overline{Z}}_T\left(\overline{\overline{T}}_J + \overline{\overline{G}}_2\overline{\overline{Z}}_T\right)^{-1}\left(\overline{\overline{Y}}_T + \overline{\overline{G}}_2\overline{\overline{T}}_E\right) & \overline{\overline{Z}}_T\left(\overline{\overline{T}}_J + \overline{\overline{G}}_2\overline{\overline{Z}}_T\right)^{-1} \end{bmatrix}. \tag{A10}$$

ACKNOWLEDGMENT

The authors wish to thank T. Plunk, J. Mather, and J. Robinson for their help during the course of this project.

REFERENCES

[1] G. Böck, "New multilayered slot line structures with high nonreciprocity," *Electron. Lett.*, vol. 19, no. 23, pp. 966–968, Nov. 1983.

[2] M. Geshiro and T. Itoh, "Analysis of double layered finlines containing a magnetized ferrite," in *IEEE MTT Int. Microwave Symp. Dig.*, 1986, pp. 743–744.

[3] G. Robinson and J. Allen, "Slot line application to miniature ferrite devices," *IEEE Trans. Microwave Theory Tech.*, vol. MTT-17, pp. 1037–1101, Dec. 1969.

[4] E. El-Sharawy and R. W. Jackson, "Coplanar waveguide and slot line on magnetic substrates: Analysis and experiment," *IEEE Trans. Microwave Theory Tech.*, vol. 36, pp. 1071–1079, June 1988.

[5] J. Minor and M. Bolle, "Modes in the shielded microstrip on a ferrite substrate transversely magnetized in the plane of the substrate," *IEEE Trans. Microwave Theory Tech.*, vol. MTT-19, pp. 570–577, July 1971.

[6] T. Kaneki, "Phase constants of the slot line and coplanar waveguide with ferrite substrates," *Denshi Trushin Gakki Robunski*, vol. 55, pp. 21–22, 1972.

[7] F. Lange, "Analysis of shielded strip and slot lines on a ferrite substrate transversely magnetized in the plane of the substrate," *Arch. Elek. Übertragung.*, Band 36, Heft 3, pp. 95–100, Mar. 1982.

[8] R. Pregla and S. Worm, "A new technique for the analysis of planar waveguides with magnetized ferrite substrate," in *Proc. European Microwave Conf.* (Helsinki), 1982, pp. 747–752.

[9] T. Itoh, "Spectral domain immittance approach for dispersion characteristics of generalized printed transmission lines," *IEEE Trans. Microwave Theory Tech.*, vol. MTT-28, pp. 733–736, 1980.

[10] E. Riches, P. Brennan, P. Brigginshaw, and S. Deeley, "Microstrip ferrite devices using surface field effects for microwave integrated circuits," *IEEE Trans. Magn.*, vol. MAG-6, pp. 670–673, Sept. 1970.

[11] E. El-Sharawy, Ph.D. thesis, University of Massachusetts, Amherst, MA, 1989.

[12] W. P. Clark, "A technique for improving the figure-of-merit of a twin slab nonreciprocal phase shifter," *IEEE Trans. Microwave Theory Tech.*, vol. MTT-16, pp. 974–975, Nov. 1968.

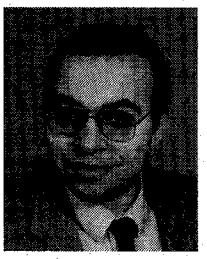

El-Badawy El-Sharawy (S'85–M'89) was born on October 18, 1957, in Mansoura, Egypt. He received the B.Sc. and M.Sc. degrees (with honors) from Mansoura University, Egypt, in 1980 and 1984, respectively, and the Ph.D. degree from the University of Massachusetts, Amherst, in 1989, all in electrical engineering.

He joined Arizona State University in 1989, where he is currently an Assistant Professor of Electrical Engineering. His research interest is in the area of analysis and design of ferrite devices. Dr. El-Sharawy is a member of Eta Kappa Nu.

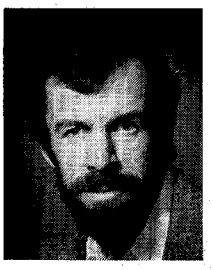

Robert W. Jackson (M'82–SM'88) was born in Boston, MA, in 1952. He received the B.S. (1975), M.S. (1979), and Ph.D. (1981) degrees in electrical engineering from Northeastern University, Boston, MA. His dissertation was concerned with nonlinear plasma interactions in the bow shock of the earth.

From 1981 to 1982, he was an Assistant Professor in the Department of Electrical Engineering at Northeastern University. Since 1982, he has been on the faculty of the Department of Electrical and Computer Engineering at the University of Massachusetts at Amherst, where he is currently an Associate Professor. His research interests include the electromagnetic aspects of integrated circuits, novel printed circuit and antenna structures, the modeling and design of planar ferrite devices, electromagnetics applied to nonlinear or anisotropic materials, and active microwave circuit design.